Bull. Mater. Sci., Vol. 40, No. 6, October 2017, pp. 1171–1178
DOI 10.1007/s12034-017-1474-1

Enhanced infrared transmission characteristics of microwave-sintered Y_2O_3–MgO nanocomposite

C T MATHEW, SAM SOLOMON, JACOB KOSHY and JIJIMON K THOMAS*
Electronic Materials Research Laboratory, Department of Physics, Mar Ivanios College, Thiruvananthapuram 695015, India
*Author for correspondence (jkthomasemrl@yahoo.com)

MS received 29 June 2016; accepted 20 February 2017; published online 22 September 2017

Abstract. Infrared (IR) transparent ceramics are found to have applications in demanding defence and space missions. In this work, Y_2O_3–MgO nanocomposites were synthesised by a modified single-step combustion technique. The characterisation of the as-prepared powder by X-ray diffraction and transmission electron microscopy revealed the presence of cubic phases of ultra-fine nanostructured Y_2O_3 and MgO, with an average crystallite size of ∼19 nm. For the first time the resistive and microwave heatings were effectively coupled for sintering the sample, and it was found that the sintering temperature and soaking time were reduced considerably. The pellets were sintered to 99.2% of the theoretical density at 1430°C for a soaking duration of 20 min. The well-sintered pellets with an average grain size of ∼200 nm showed better transmittance properties relative to pure yttria. The promising percentage transmission of 80% in the UV–visible region and 82% in the mid-IR region shown by Y_2O_3–MgO nanocomposites can be tailored and made cost-effective to fabricate high-quality IR windows for strategic defence and space missions.

Keywords. Nanocomposites; infrared transparent window; hybrid sintering; transmittance; combustion synthesis.

1. Introduction

For the last few decades, researchers have been exhaustively working for improving the transmittance properties of the existing infrared (IR) transparent ceramics, along with the search of finding new polycrystalline materials for making high-quality IR-transparent windows due to their high-demand applications in the strategic defence and space missions [1,2]. In addition to these, IR-transparent ceramics are found to have a wide spectrum of civilian applications as well [3–6].

A large variety of IR-transparent materials have so far been developed, but the technologists are forced to compromise between different properties that adversely affect the performance of the IR windows and domes. As an example, a single-crystal sapphire is a proven IR-transparent material with high-end durability and mechanical strength as well, but the IR cut-off wavelength and machinability are found to be low, in addition to the high cost of production [1]. On the other hand, using a polycrystalline material, the production cost can be minimised extensively and the preferred optical, thermal, mechanical and electrical properties can be achieved to a greater extent. However, in the case of these polycrystalline ceramics, the sintering of the sample to full density with minimum grain size and without any pores sets barriers to the fabrication and it impedes the preferred applications. A large quantum of works has been reported in literatures using polycrystalline cubic phase Y_2O_3, $MgAl_2O_4$ and MgO, yielding transparent windows for practical applications due to their isotropic nature [7–9]. Among them, Y_2O_3 and MgO have gained a distinctive attention due to their large IR cut-off, high melting point and high transmittance percentage in the mid-IR range [1]. The desired mechanical, thermal and electrical properties, in addition to the high IR cut-off, make them ideal for IR windows and protection domes used in strategic applications.

It is quite evident that high quality of the starting powder is essential for the fabrication of high-performance IR-transparent windows [1]. Various techniques are available in the literature for synthesising ultra-fine yttria [10,11] and magnesia [12,13]. Fabrication methods like flame spray pyrolysis [14], sol–gel combustion [15,16], esterification sol–gel route [17], etc. have been successfully employed to prepare ultra-fine nanostructured yttria–magnesia nanocomposites. Combustion syntheses of many ceramic powders including nanomaterials have been widely studied and reported in literatures [18–20]. However, this synthesis technique has not been explored fully so far in detail in the case of IR-transparent ceramics. In combustion synthesis, an exothermic redox chemical reaction is used to produce useful materials [20]. This process is attractive and popular among the researchers in manufacturing technologically useful materials at lower cost, because it employs relatively low-cost equipment, has very short processing time and yields high-purity products.

Sintering of the sample to high density plays a vital role in the fabrication of any IR-transparent window [1]. Sintering

the samples at relatively low temperature with minimum soaking duration will yield high-quality transparent ceramics with reduced grain size and minimum porosity [21,22]. Literatures reveal that well-sintered pellets with grain size less than that of the IR wavelength in consideration will improve the mechanical properties and transmittance [23–25]. Y_2O_3 and MgO have been synthesised using solid-state synthesis techniques, but the sintering temperature was above 1700°C for both of the micron-sized starting powders [26,27]. Synthesis as nanopowders using the combustion technique resulted in the sintering of the obtained nanopowders at a lower temperature ∼1600°C [21]. The slow heating and the prolonged soaking duration in conventional sintering methods result in grain growth, which adversely influences the transmission characteristics. Hence, the processing methods that hinder grain growth and reduce porosity are required for fabricating high-quality windows. The presence of a second phase in the sample will also hinder the grain growth considerably by the zener pinning mechanism [28]. However, the difference in refractive indices of the phases will result in reduced transmittance and hence researchers are forced to focus selectively on single-phase systems with a cubic structure [1]. In recent years, a few works were reported in the fabrication of yttria–magnesia nanocomposites using spark plasma sintering (SPS) mechanism to address the challenges in the field of nanocomposites [24,29]. SPS yields better performing windows with reduced grain size and good transmittance. However, the processing conditions were complex; the as-sintered pellet showed a transmittance of 71% and a post-sinter annealing of 15 h yielded 80% transmittance [24]. Pressure-less sintering followed by hot isostatic press, and post-sinter annealing of 10 h, was also employed for getting highly dense yttria–magnesia composites [16], but the transmittance percentage was relatively low. Microwave sintering has now evolved as an alternative for SPS, to fabricate IR-transparent windows [30]. Very recently, we synthesised and sintered Y_2O_3 and $MgAl_2O_4$ nanopowders using an integrated resistive and microwave heating using hybrid microwave heating with significantly improved characteristics [21,22]. Sintering kinetics of Y_2O_3–MgO composite using microwave heating are available in the literature [31]. However, to the best of our knowledge, no studies have so far been reported on sintering the Y_2O_3–MgO nanocomposites using resistive microwave hybrid heating. Hybrid sintering is a promising mechanism in which resistive and microwave heatings are coupled in a desired proportion to yield highly dense ceramics with reduced grain size and minimum porosity. It is a simple mechanism where there is no complex step involved in sample preparation and application of microwave energy, and is economical in terms of time, energy and cost.

In the present work, a single-step modified combustion synthesis [32,33] developed by us has been used as an effective technique for the synthesis of phase-pure nanoparticles of yttria–magnesia nanocomposites of particle size (5–25 nm). The greatest advantage of this relatively simple method is that without high temperature calcinations for prolonged duration, we could obtain yttria–magnesia nanocomposites of extremely small size. The nano-powder with high sinterability is further compacted to an optimum density at a much lower sintering temperature using a hybrid heating technique yielding samples with high thermal stability and good transparency to IR radiations. The structure, vibrational spectra surface morphology, transmittance characteristics of the sintered pellets in the mid-IR range and UV–visible range have also been studied and reported

2. Experimental

A single-step auto-igniting combustion synthesis was used to prepare nano-structured yttria [20]. Stoichiometric amounts of high-purity metal salts of Y and M, namely $Y(NO_3)_3 \cdot 6H_2O$ (99.99%, Alfa Aesar, USA) and $Mg(NO_3)_2 \cdot 6H_2O$ (99.99%, Alfa Aesar, USA), respectively, were dissolved in double-distilled water in the volume ratio of 50:50 of the oxides to make a clear solution. The amount of citric acid, which is used as the complexing agent, was calculated based on the total valence of the oxidising and the reducing agents for maximum release of energy during combustion [19]. Nitric acid was used as the oxidising agent, and ammonia as the fuel and the pH of the solution was monitored till it became ∼7. The solution containing the precursor mixture was heated using a hot plate at 250°C in a ventilated fume hood. The solution boils on heating and undergoes dehydration accompanied by foam. The foam then ignites by itself on persistent heating, giving voluminous and fluffy product of combustion.

The as-prepared Y_2O_3–MgO nanocomposite obtained in the combustion process was analysed by different powder characterisation techniques. As-prepared samples were characterised by an X-ray diffractometer (X'pert pro, Philips, the Netherlands) with Cu Kα radiation in the range of 20–60° in steps of 0.0840° for the determination of crystalline structure and phase of the nanomaterials. The average crystallite size was estimated for all the samples using Scherrer's equation. The Wiliamson–Hall (W–H) plot was used for studying the lattice strain in the sample. Particulate properties of the combustion product were examined using high-resolution transmission electron microscopy (HRTEM; H600, Hitachi, Japan) operated at 200 kV. The samples for transmission electron microscopy (TEM) were prepared by ultrasonically dispersing the powder in methanol and allowing a drop of this to become dry on a carbon-coated copper grid. Additional information regarding the phase purity and the presence of any inorganic impurity was obtained from Fourier transform infrared (FTIR) spectroscopy taken using an FTIR spectrometer (Spectrum 2, Perkin-Elmer, Singapore) in the range 400–4000 cm^{-1} using the ATR method. The absorption spectrum of as-prepared samples of yttria nanoparticles was recorded using a spectrophotometer (UV-1700, Shimadzu, Singapore). The thermal properties of the powder were studied using a Perkin-Elmer TGA–DTA thermal analyser.

The as-prepared powder was uniaxially compacted into pellets in a 14 mm diameter steel die at 20 MPa using a hydraulic press. The sintering of the disc-shaped pellets was carried out in a resistive–microwave hybrid furnace with silicon carbide susceptors (VBCC/HMF/71,VB Ceramics Consultants, India). In the hybrid furnace, microwave heating was realised using a pair of 2.45-GHz magnetrons, each of 1.1 kW, and for resistive heating, a pair of molybdenum disilicide heating elements was used. The experimental density of the sintered pellets was calculated using the Archimedes principle. The surface morphological studies of the sintered pellets were performed by scanning electron microscopy (SEM; 6390LV, JEOL, Japan). Digimizer (version 4.6.1) software was used for grain size analysis. The transmittances of radiation in the UV–visible and in the IR range were measured using UV–visible and FTIR spectrometers.

3. Results and discussion

X-ray diffraction (XRD) analysis of the as-prepared Y_2O_3–MgO nanocomposite is shown in the figure 1a. The XRD analysis reveals that the as-prepared powder is composed of cubic Y_2O_3 (JCPDS: 89-5591) and MgO (JCPDS: 65-0476) phases, and the results confirm the formation of yttria and magnesia nanoparticles by the auto-ignited single-step modified combustion synthesis without post-annealing or calcination.

The average crystallite size was calculated using the Scherrer formula [34] $D = 0.9\lambda/(\beta \cos\theta)$, where λ is the wavelength of CuKα radiation, β is the full-width at half-maximum and θ is the Bragg's diffraction angle. The crystallites were found to be in the size range of 15–25 nm and the average size of the crystallites was 19.0 nm. The crystallite size calculated from the high-intensity peak corresponding to the (222) plane of Y_2O_3 was 16.2 nm, and d-spacing was 0.3029 nm. The peak corresponding to (220) plane of MgO was also identified and the crystallite size was calculated as 16.5 nm with the d-spacing of 0.1484 nm. All the d-spacing values are in good agreement with the JCPDS records. These results show that the single-step combustion method employed in the present study offers an excellent and economical mode for the preparation of phase-pure ultrafine yttria–magnesia nanocomposite.

The Williamson–Hall (W–H) method was used to find out the extent of line broadening in the diffraction pattern due to the strain, which occurs by the non-uniform displacement of the atoms with respect to their reference lattice position [35]. In this method, the reciprocal peak width $(\beta \cos\theta)/\lambda$ is plotted against the reciprocal lattice distance $(\sin\theta)/\lambda$; the resulting plot was linearly fit. Figure 1b shows the W–H plot for the yttria–magnesia nanocomposites. The reciprocal of y intercept, a measure of crystallite size, obtained from this plot was 22.2 nm. The lattice strain constant η, proportional to the slope of the line, was estimated at 1.154×10^{-4}. The positive slope of the line indicates tensile strain, and it is also a component contributing to the broadening of peaks in the XRD pattern.

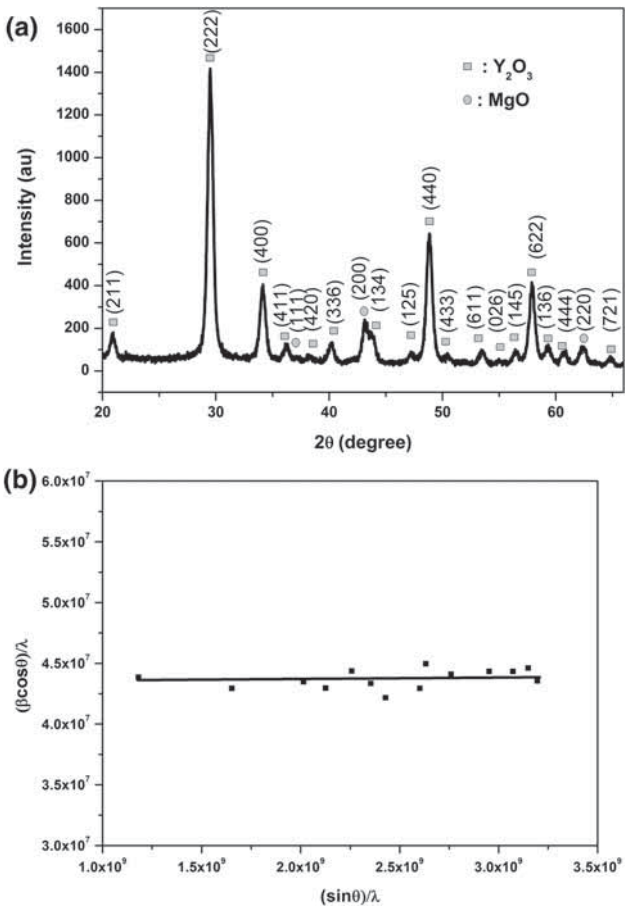

Figure 1. (**a**) XRD pattern of as-prepared Y_2O_3–MgO nanocomposite. (**b**) Wiliamson–Hall plot of as-prepared nano Y_2O_3–MgO nanocomposite.

Figure 2a shows the TEM image of the as-prepared nanocomposites. The TEM image reveals that the crystallites are in the size range 12–24 nm. Figure 2b shows the different crystallographic planes of Y_2O_3–MgO nanocomposites, and from the distinctly visible grain, the crystallite size was calculated as 15.6 nm, corresponding to the (222) plane of cubic crystal structure of yttria. The d-spacings obtained from the HRTEM are in good agreement with those obtained from XRD analysis, which match very well with the JCPDS values. The HRTEM also supports the presence of Y_2O_3 and MgO phases in the as-prepared powder.

The vibrational spectra of the samples were examined by FTIR spectral analysis. The FTIR spectrum of the powder in figure 3a shows characteristic vibrations of both Y_2O_3 and MgO. The absorption peaks at 558 and 850 cm^{-1} correspond to Y–O stretching [36]. The bands at 462 cm^{-1} correspond to typical stretching vibration of metal–oxygen bonds in yttria and magnesia [36,37]. The small peak at 850 cm^{-1} and the shoulder at 700 cm^{-1} are due to the M–O bonds [38]. A broad

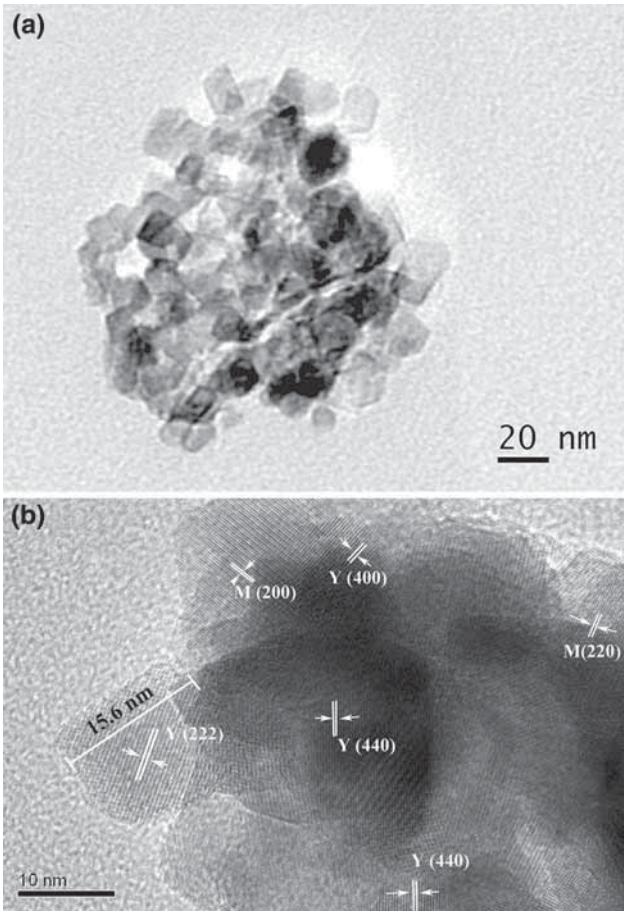

Figure 2. (**a**) TEM image of as-prepared nano Y_2O_3–MgO nanocomposite. (**b**) HRTEM image of different crystallographic planes.

absorption peak around 3400 and 1661 cm^{-1} are the O–H stretching and H–O–H bending modes, respectively, of the molecular water adsorbed by the powder. No other absorption peaks are observed in this range, which shows that no residual nitrate or other impurities are present in the as-prepared powder.

The UV–visible absorption spectrum was recorded in the range 200–800 nm and is shown in figure 3b. The maximum absorption triggered at 214 nm is due to the excitation of the electrons from the top of the valence band to the bottom of the conduction band. The optical band gap energy was determined by extrapolating the wavelength of the onset absorption in the UV region using the intercept in the wavelength axis. The corresponding band gap (E_g) for the 214 nm wavelength is 5.80 eV. The result shows that the as-prepared sample is a wide-band-gap material, which heavily absorbs in the high-frequency UV region and finds applications also in the UV sensors and filters. The maximum absorption is at 214 nm, which confirms the suitability of the material to be used as a potential candidate for UV filters, which screen hazardous high energies of the ultraviolet spectrum from 10 to 120 nm that cause biological damage, and it also finds application as microwave filters.

The measured reflectance is converted into the Kubelka–Munk function $F(R) = (1 - R)^2/(2R)$, where R is the reflectance. The K–M function is proportional to the absorption coefficient α in the Tauc equation [39,40]. Using the K–M function, $(F(R)h\upsilon)^2$ is plotted against $h\upsilon$ in figure 3c. The optical band gap energy can be obtained from the intercept of the linear region with the energy axis at $(F(R)h\upsilon)^2 = 0$); it is found to be 5.82 eV and it can be used to calculate the refractive index of the sample.

The refractive index of the material is a fundamental property, which is closely related to the electronic polarisability and local field inside the material. If the particle size of the sample is small, the band gap energy will be high and the refractive index corresponding to it will be low. Based on the empirical relationship $E_g e^n = 36.3$ between the refractive index (n) and band gap energy (E_g) developed by Reddy and Anjaneyulu [41], the refractive index of the ultrafine sample is calculated as 1.83 from the powder with band gap 5.82 eV; the theoretical limit of transmittance in the UV–visible range for a well-sintered pellet using the powder will be 84.15% according to the relation $T = 2n/(1 + n^2)$ [1] and is found to be in close agreement with earlier reports [14].

The thermal stability of the yttria–magnesia composite powder synthesised via modified combustion synthesis is analysed using TGA and DTA curves shown in figure 4. A weight loss of ∼10% in the TGA curve below 600°C is due to the presence of adsorbed water and the organic matter present in the combustion synthesised powder. The endothermic dip in the DTA curve at 100°C accounts for the expulsion of adsorbed water from the sample. Above 600°C there is no evidence of weight loss in the TGA or any abrupt change in the DTA, which indicates that there is no phase transition, and the sample is stable at elevated temperature, which is counted as a prerequisite for window materials used in demanding missions at elevated temperatures.

The yttria–magnesia composite powder was uniaxially compacted into pellets in a 14 mm diameter steel die at 20 MPa using a hydraulic press. The sintering behaviour of the sample was studied using resistive–microwave hybrid heating and compared with the resistive heating in conventional sintering. Figure 5a shows the variation in relative density and the densification rate (derivative of relative density with temperature) with sintering temperature during conventional sintering. The effective densification starts around 1250°C and peaks around 1430°C. The pellet achieved a density of 98.1% of the theoretical density at 1600°C for a soaking duration of 2 h. The heating rate employed is 10°C min^{-1}. Heating rate above this generated cracks in the sample. However, in samples of hybrid sintering shown in figure 5b, it is clear that the effective densification starts around 1150°C and the maximum densification rate is observed around 1380°C. In the hybrid furnace, the pellets were heated at a constant rate of 40° C min^{-1} and could be sintered to an optimum value of 99.2% of the theoretical density at a much lower

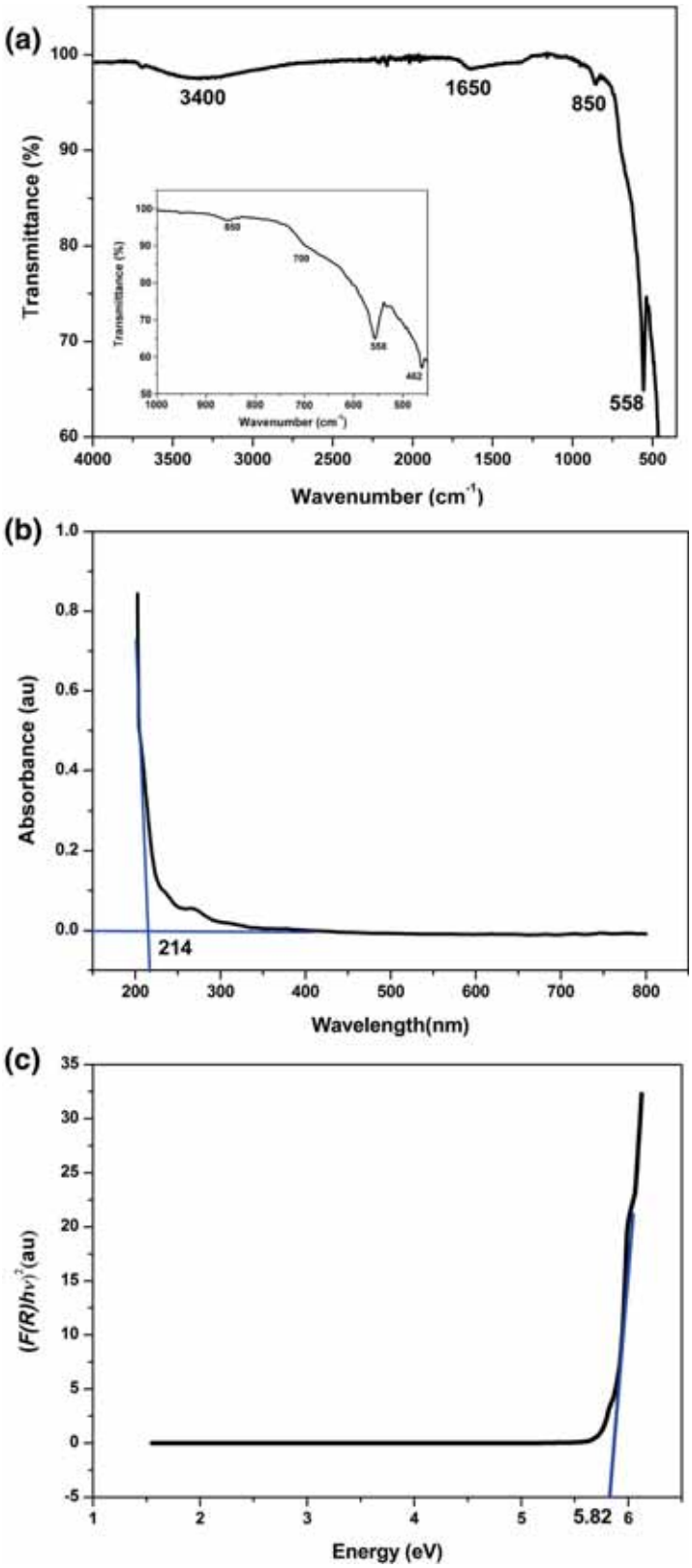

Figure 3. (**a**) FTIR spectrum of as-synthesised Y_2O_3–MgO composite. The characteristic peaks are shown in the inset. (**b**) UV–visible absorption spectrum of as-prepared Y_2O_3–MgO composite. (**c**) Tauc's plot in terms of Kubelka–Munk function.

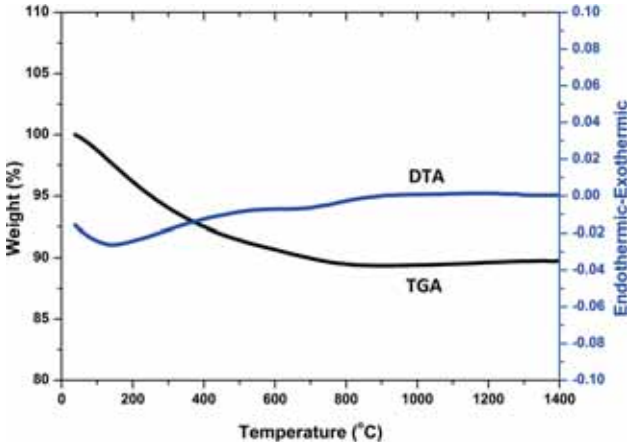

Figure 4. TGA and DTA curves of as-synthesised Y_2O_3–MgO composite powder.

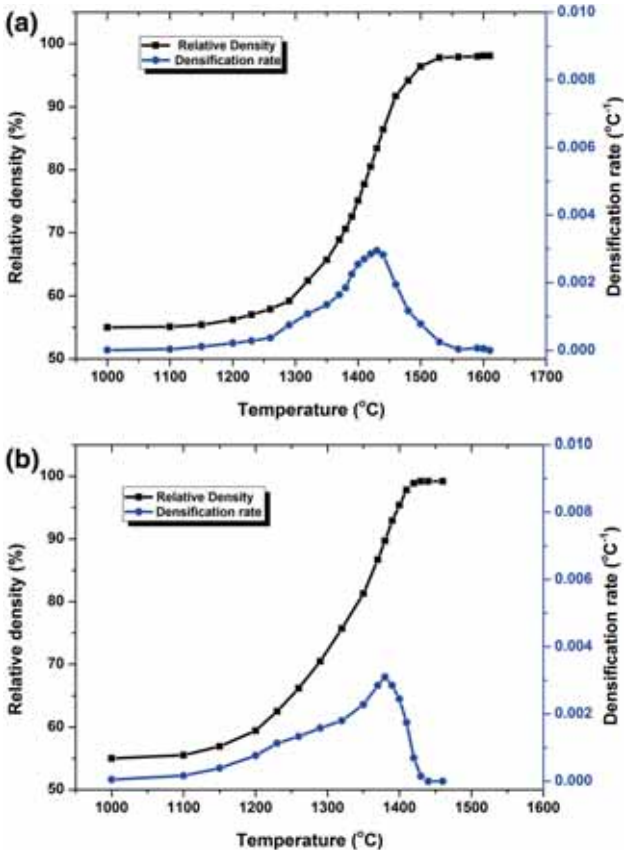

Figure 5. Variation of relative density and densification rate of the sample with sintering temperature in (**a**) conventional sintering and (**b**) hybrid sintering.

temperature of 1430°C with soaking time of only 20 min for the first time. It is found that the sintering temperature is reduced considerably in resistive–microwave hybrid heating. In hybrid heating the sample pellet obtains heat from the microwaves generated simultaneously from the magnetrons and molybdenum heating elements, which enhances the densification to a great extent. To optimise the sintering strategy, a series of sintering trials were done by coupling different percentages of microwave heating and resistive heating, and the details are found elsewhere [21]. At low temperature the surface diffusion is high, which will not contribute to the shrinkage [42]. Remarkable sintering enhancement compared with the conventional sintering was observed in our previous studies as well [21,22]. A uniform distribution of heat energy towards the green pellet is a consequence of the effective coupling of resistive and microwave heatings, leading to enhancement of grain boundary diffusion, which in turn improves the sintering process. In the present case, the hybrid sintering behaviour was highly effective when 60% resistive heating and 40% microwave heating were coupled up to 1100°C and 40% resistive heating and 60% microwave heating were employed from 1100 to 1430°C. In this consistent distribution of thermal energy, we were able to sinter the sample to >99% of the theoretical density with an average grain size of ∼200 nm. Hybrid sintering is hence found to be a promising sintering method, effectively promoting the densification of yttria–magnesia composite at a lower temperature.

The highly dense sintered pellets were hand polished, followed by thermal etching at 1330°C for an hour in air. The surface morphology of the sintered samples was studied using SEM. Figure 6a is a SEM micrograph of the pellet sintered via hybrid heating, which indicates that the pellet is well sintered with minimum porosity. The light phase in the SEM image corresponds to yttria and the dark phase corresponds to magnesia [16]. The grain size distribution in the matrix is shown in figure 6b. In the pellet sintered by hybrid heating, maximum number of grains lie in the size range 0.1–0.3 μm and the average grain size of the entire distribution is ∼200 nm. The reduced grain size in the hybrid sintered pellet is a remarkable result, which can be successfully used in the fabrication of highly transparent windows without compromising on the mechanical strength.

The hand-polished pellets were further lapped and polished using diamond pastes of fine grades in a self-designed lapping and polishing machine and the final mirror polished pellets were used for the transmittance studies. Figure 7 shows the transmittance spectra of the sintered pellets of 0.5 mm thickness in the UV–visible region. The pellet sintered through resistive microwave hybrid heating shows a maximum transmittance of 80% at 800 nm. This improvement of the transmittance in this case attributes to the enormous reduction in grain size and tight packing of the grains. Moreover, as the grain growth is inhibited due to the fast heating rate of hybrid heating and the zener pinning effect due to the second phase, lead to very low scattering resulting improvement in the transmittance percentage. The photographs of the pellet sintered to 99.2% theoretical density using hybrid heating is shown in the inset of figure 7. The pellet of thickness 0.5 mm is kept 2 mm above a computer screen and is found to be translucent.

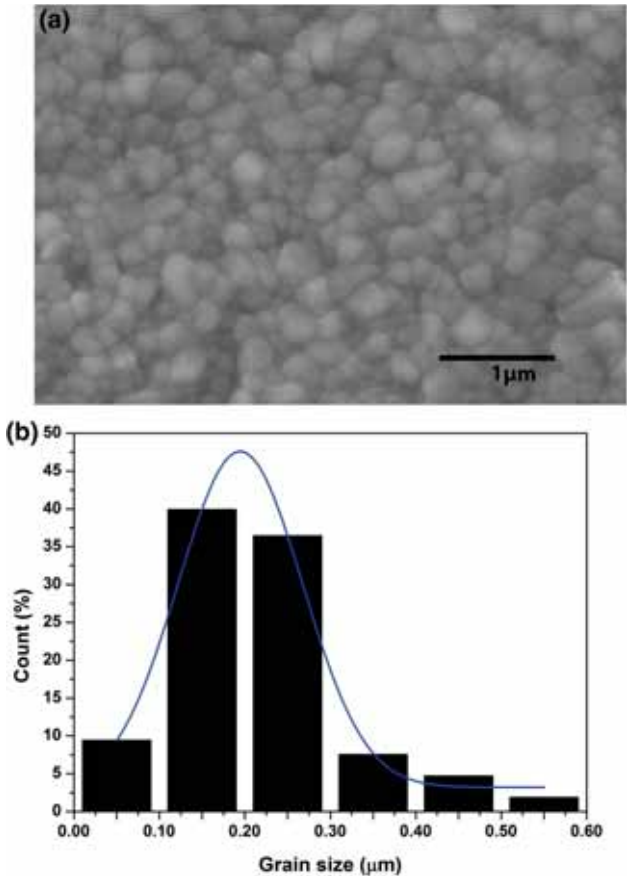

Figure 6. (**a**) SEM micrographs of the pellet. (**b**) Grain size distribution in the sintered pellet.

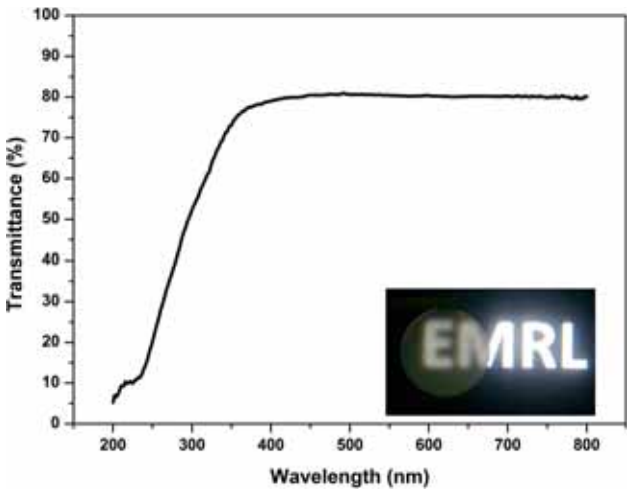

Figure 7. UV–visible transmittance spectrum of sintered pellet. Inset: photograph of the Y_2O_3–MgO composite.

The IR transmittance spectrum of the pellet sintered using resistive-microwave hybrid heating is shown in figure 8. It shows that the well-sintered pellet has a maximum transmittance of 82% at 5 μm. The transmittance obtained in the present work is relatively high compared with the most recent reports [17] and that obtained for pure yttria via microwave hybrid sintering [21].

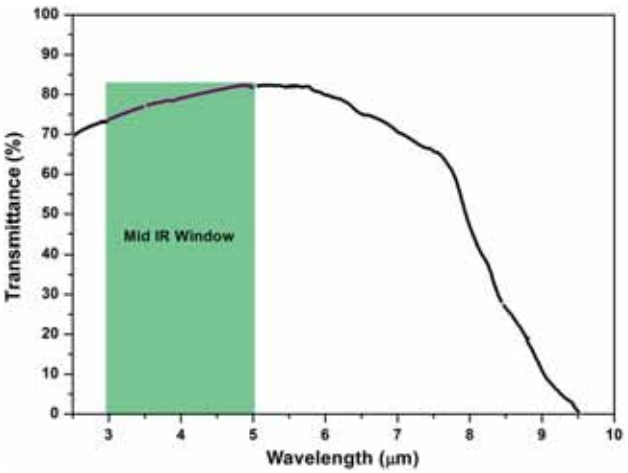

Figure 8. IR transmittance spectrum of Y_2O_3–MgO composite pellet sintered to 99.2% of theoretical density.

The high sinterability of the yttria–magnesia nanocomposite synthesised using the modified combustion synthesis and the effective coupling of resistive and microwave heating during sintering substantially reduces the sintering temperature. The fast heating, the short soaking duration and the pinning effects in the composites hinder the grain growth and reduce the porosity. The machine polishing of the well-sintered pellet using diamond paste of fine grade with high surface finish results in the reduction of surface scattering. The excellent transmittance in the mid-IR range makes it ideal for IR-transparent windows and domes.

4. Conclusions

Nanostructured Y_2O_3–MgO composite powders were successfully synthesised by a single-step auto-igniting combustion technique with an average crystallite size of ∼19 nm. The compacted pellets of the nanocomposite were densified via hybrid sintering, which effectively couples the resistive and microwave heating in definite proportion. A substantial reduction in sintering temperature to 1430°C for a soaking duration of 20 min was observed. The well-sintered pellet with reduced average grain size of ∼200 nm showed enhanced transmittance of 80% in the visible and 82% in the mid-IR region. The promising results obtained in the present work are the combined effect of the modified combustion synthesis, resistive microwave hybrid sintering and mirror quality surface finish. The results clearly indicate that the modified single-step combustion technique is a promising method to synthesise nanocomposites and the hybrid sintering is an effective technique to fabricate high-quality IR-transparent windows with enhanced properties.

Acknowledgements

This work is supported by the Department of Science and Technology Science and Engineering Research Board, Government of India, under Grant Number SB/S2/CMP-0021/2013.

References

[1] Harris D C 1999 *Materials for infrared windows and domes: properties and performance* (Bellingham, WA: SPIE Press)
[2] Grujicic M, Bell W C and Pandurangan B 2012 *Mater. Des.* **34** 808
[3] Lan Y H, Jun J Z, Jian M X and Wei W S 2010 *J. Inorg. Mater.* **25** 795
[4] Qin X, Yang H, Shen D, Chen H, Zhou G, Wang S *et al* 2013 *Int. J. Appl. Ceram. Technol.* **10** 123
[5] Tetsui T, Kobayashi T, Mori T, Kishimoto T and Harada H 2010 *Mater. Trans.* **51** 1656
[6] Silva D D and Boccaccini A R 2008 *Recent Pat. Mater. Sci.* **1** 56
[7] Wen L, Sun X, Lu Q, Xu G and Hu X 2006 *Opt. Mater.* **29** 239
[8] Wang C and Zhao Z 2009 *Scr. Mater.* **61** 193
[9] Fang Y, Agrawal D, Skandan G and Jain M 2004 *Mater. Lett.* **58** 551
[10] Huang Z, Sun X, Xiu Z, Chen S and Tsai C T 2004 *Mater. Lett.* **58** 2137
[11] Srinivasan R, Yogamalar R and Bose A C 2010 *Mater. Res. Bull.* **45** 1165
[12] Ganguly A, Trinh P, Ramanujachary K V, Ahmad T, Mugweru A and Ganguli A K 2011 *J. Colloid Interface Sci.* **353** 137
[13] Makhulf S, Dror R, Nitzan Y, Abramovich Y, Jelinek R and Gedanken A 2005 *Adv. Funct. Mater.* **15** 1708
[14] Harris D C, Cambrea L R, Johnson L F, Seaver R T, Boronowski M, Gentilman R *et al* 2013 *J. Am. Ceram. Soc.* **96** 3828
[15] Wang J, Zhang L, Chen D, Jordan E H and Gell M 2012 *J. Am. Ceram. Soc.* **95** 1033
[16] Wang J, Chen D, Jordan E H and Gel M 2010 *J. Am. Ceram. Soc.* **93** 3535
[17] Xu S, Li J, Kou H, Shi Y, Pan Y and Guo J 2015 *Ceram. Int.* **21** 3312
[18] Thomas J K, Padma Kumar H, Pazhani R, Solomon S, Jose R and Koshy J 2007 *Mater. Lett.* **61** 1592
[19] Thomas J K, Padma Kumar H, Solomon S, George C N, Joy K and Koshy J 2007 *Phys. Status Solidi (a)* **204** 3102
[20] Thomas J K, Padma Kumar H, John Annamma, Suni V, Joy K, Solomon S *et al* 2009 *J. Phys. Chem. Solids* **70** 703
[21] Mathew C T, Solomon S, Koshy J and Thomas J K 2015 *Ceram. Int.* **41** 10070
[22] Mathew C T, Vidya S, Koshy J, Solomon S and Thomas J K 2015 *Infrared Phys. Technol.* **72** 153
[23] Aksel C and Riley F L 2003 *J. Eur. Ceram. Soc.* **23** 307
[24] Jiang D T and Mukherjee A K 2010 *J. Am. Ceram. Soc.* **93** 769
[25] Meyers M A, Mishra A and Benson D J 2006 *Prog. Mater. Sci.* **51** 427
[26] Tsukuda Y and Muta A 1976 *J. Ceram. Soc. Jpn.* **84** 585
[27] Wilde G 2009 *Nanostructured materials* (Kidlington, UK: Elsevier)
[28] Couturier G, Doherty R, Maurice C and Fortunier R 2005 *Acta Mater.* **53** 977
[29] Huang L, Yao W, Liu J, Mukherjee A K and Schoenung J M 2014 *Scr. Mater.* **75** 18
[30] Luo J, Zhong Z and Xu J 2012 *Mater. Res. Bull.* **47** 4283
[31] Sun H, Zhang Y, Gong H, Li T and Li Q 2014 *Ceram. Int.* **40** 10211
[32] James J, Jose R, John A M and Koshy J 2004 *A single step process for the synthesis of nanoparticles of ceramic oxide powders* US Patent 6761866
[33] James J, Jose R, John Asha M and Koshy J 2004 *A single step process for the synthesis of nanoparticles of ceramic oxide powders* US Patent 6835367
[34] Langford J I and Wilson A J C 1978 *J. Appl. Crystallogr.* **11** 102
[35] Williamson G K and Hall W H 1953 *Acta Metall. Mater.* **1** 22
[36] Repelin Y, Proust C, Husson E and Beny J M 1995 *J. Solid State Chem.* **118** 163
[37] Krishnamoorthy K, Moon J Y, Hyun H B, Cho S K and Kim S J 2012 *J. Mater. Chem.* **22** 24610
[38] Gourley J T and Runciman W A 1973 *J. Phys. C: Solid State* **6** 583
[39] Kubelka P 1948 *J. Opt. Soc. Am.* **38** 448
[40] Yang L, Kruse B È and Miklavcic S J 2004 *J. Opt. Soc. Am. A* **21** 1942
[41] Reddy R R and Anjaneyulu S 1992 *Phys. Status Solidi (b)* **174** 1091
[42] Rahman M N 2007 *Sintering of ceramics* (Boca Raton: CRC Press)